Vapor-Phase Processing of Metal−Organic Frameworks

Pengcheng Su, Min Tu,* Rob Ameloot,* and Wanbin Li*

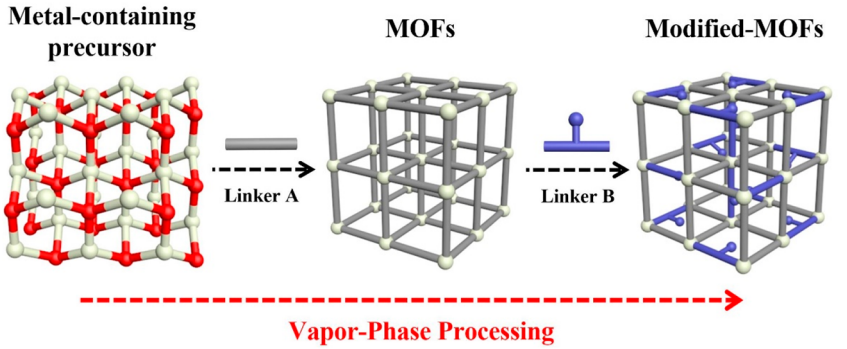

CONSPECTUS: Porous metal−organic frameworks (MOFs), formed from organic linkers and metal nodes, have attracted intense research attention. Because of their high specific surface areas, uniform and adjustable pore sizes, and versatile physicochemical properties, MOFs have shown disruptive potential in adsorption, catalysis, separation, etc. For many of these applications, MOFs are synthesized solvothermally as bulk powders and subsequently shaped as pellets or extrudates. Other applications, such as membrane separations and (opto)electronics, require the implementation of MOFs as (patterned) thin films. Most thin-film formation methods are adapted from liquid-phase synthesis protocols. Precursor transport and nucleation are difficult to control in these cases, often leading to particle formation in solution. Moreover, the use of solvents gives rise to environmental and safety challenges, incompatibility issues with some substrates, and corrosion issues in the case of dissolved metal salts. In contrast, vapor-phase processing methods have the merits of environmental friendliness, control over thickness and conformality, scalability in production, and high compatibility with other workflows.

In this Account, we outline some of our efforts and related studies in the development and application of vapor-phase processing of crystalline MOF materials (MOF-VPP). We first highlight the advances and mechanisms in the vapor-phase deposition of MOFs (MOF-VPD), mainly focusing on the reactions between a linker vapor and a metal-containing precursor layer. The characteristics of the obtained MOFs (thickness, porosity, crystallographic phase, orientation, etc.) and the correlation of these properties with the deposition parameters (precursors, temperatures, humidity, post-treatments, etc.) are discussed. Some in situ characterization methods that contributed to a fundamental understanding of the involved mechanisms are included in the discussion. Second, four vapor-phase postsynthetic functionalization (PSF) methods are summarized: linker exchange, guest loading, linker grafting, and metalation. These approaches eliminate potential solubility issues and enable fast diffusion of reactants and guests as well as a high loading or degree of exchange. Vapor-phase PSF provides a platform to modify the MOF porosity or even introduce new functionalities (e.g., luminescence photoswitching and catalytic activity). Third, since vapor-phase processing methods enable the integration of MOF film deposition into a (micro)fabrication workflow, they facilitate a range of applications with improved performance (low-*k* dielectrics, sensors, membrane separations, etc.). Finally, we provide a discussion on the limitations, challenges, and further opportunities for MOF-VPP. Through the discussion and analysis of the vapor-phase processing strategies as well as the underlying mechanisms in this Account, we hope to contribute to the development of the controllable synthesis, functionalization, and application of MOFs and related materials.

KEY REFERENCES

- Stassen, I.; Styles, M.; Grenci, G.; Van Gorp, H.; Vanderlinden, W.; De Feyter, S.; Falcaro, P.; De Vos, D.; Vereecken, P.; Ameloot, R. Chemical Vapour Deposition of Zeolitic Imidazolate Framework Thin Films. *Nat. Mater.* **2016**, *15*, 304−310.[1] *Chemical vapor deposition for*

crystalline microporous MOFs was realized for the first time.

- Li, W.; Su, P.; Li, Z.; Xu, Z.; Wang, F.; Ou, H.; Zhang, J.; Zhang, G.; Zeng, E. Ultrathin Metal−Organic Framework Membrane Production by Gel−Vapour Deposition. *Nat. Commun.* **2017**, *8*, 406.[2] *This work reported the gel vapor deposition of ultrathin ZIF-8 molecular sieving membranes with high gas separation performances.*
- Wu, W.; Su, J.; Jia, M.; Li, Z.; Liu, G.; Li, W. Vapor-Phase Linker Exchange of Metal−Organic Frameworks. *Sci. Adv.* **2020**, *6*, eaax7270.[3] *This work reported the vapor-phase linker exchange of ZIF-8 performed by single/multistage exchanges to tune the gas adsorption performance.*
- Tu, M.; Kravchenko, D. E.; Xia, B.; Rubio-Giménez, V.; Wauteraerts, N.; Verbeke, R.; Vankelecom, I.; Stassin, T.; Egger, W.; Dickmann, M.; Amenitsch, H.; Ameloot, R. Template-Mediated Control over Polymorphism in the Vapor-Assisted Formation of Zeolitic Imidazolate Framework Powders and Films. *Angew. Chem., Int. Ed.* **2021**, *60*, 7553−7558.[4] *This work reported control over the polymorphism of MOF thin films through the addition of template vapors.*

INTRODUCTION

Vapor-phase processing (VPP) is widely employed in micro- and nanofabrication to deposit uniform coatings with high reproducibility.[5] The scope of materials that can be deposited from the vapor phase has greatly expanded over the past decades, from traditional metals, inorganics, and organics to porous frameworks.[6] Because of their ultrahigh specific surface areas and pores with uniform size and versatile functionalities, metal−organic frameworks (MOFs) are attractive for catalysis, adsorption, separation, drug delivery, microelectronics, etc.[7−9] Most MOFs, both in powder and thin-film format, are synthesized in solution. Typical approaches include hydro/solvothermal synthesis, electrochemical deposition, layer-by-layer assembly, and interfacial synthesis.[10,11] Although these strategies enable the synthesis of various MOF powders and thin films, nucleation and growth are hard to control (e.g., leading to particle contamination due to homogeneous nucleation). In addition, using solvents causes environmental and safety concerns, and for some specific applications, e.g., microelectronics and membrane separation, corrosion due to dissolved metal salts, surface-tension-related phenomena, and undesired substrate swelling or even dissolution limit their implementation. In order to circumvent such limitations, solvent-free syntheses of MOFs have been developed. The first strategies relied on solid-state approaches, mainly through mechanochemical processing or thermal treatment of precursor mixtures.[12−14] While mechanochemical synthesis is an efficient approach for MOF powders, it is challenging to apply for thin films. Several supported MOF films and patterns have been obtained by the reaction between a metal-containing precursor layer and a melted organic linker.[15,16] However, these solvent-free approaches do not yet enable deposition of uniform and conformal MOF thin films.

Vapor-phase processing for the synthesis and deposition of MOFs (MOF-VPP) in powder and thin-film formats has been reported and has further been developed for postsynthetic functionalization of MOFs.[17−19] MOF-VPP has several advantages: (1) no or very little use of organic solvents; (2) strict limitation of deposition to the surface, avoiding particle formation due to homogeneous nucleation; (3) compatibility with substrates that are sensitive to solvents or metal salts; (4) controllable film thickness, roughness, uniformity, and conformality; (5) straightforward integration with existing facilities and manufacturing approaches in microelectronics; and (6) scalable large-area production, e.g., deposition of MOFs on a 200 mm Si wafer and 340 cm^2 polymer hollow fibers.[1,2,20−22] In this Account, we present some of our efforts and related studies on the vapor-phase deposition and postsynthetic functionalization of MOFs (Scheme 1), summarize their applications, and point out the needs for future developments.

Scheme 1. Vapor-Phase Processing of MOFs via Linker Vapor−Solid Reactions and Vapor-Phase Postsynthetic Functionalization (Linker Exchange, Guest Loading, Linker Grafting, and Metalation)

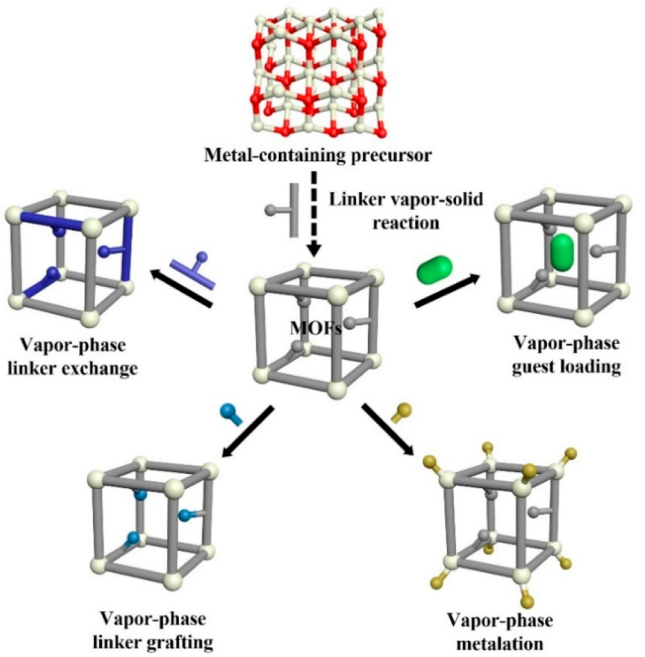

VAPOR-PHASE DEPOSITION OF MOFS

In 2016, Ameloot and co-workers developed a MOF-VPD approach to deposit uniform, continuous, and pinhole-free MOF thin films.[1] Typically, this MOF-VPD approach consists of two steps (Figure 1): (i) deposition of the metal-containing precursor layer and (ii) the vapor−solid reaction between the metal-containing precursor and the linker vapor. The first step is typically conducted through well-established vapor-phase deposition techniques such as atomic layer deposition (ALD), chemical vapor deposition (CVD), or physical vapor deposition (PVD). Relying on sequential self-limiting surface reactions, ALD enables thin-film deposition with high conformality and nanoscale control over the film thickness.[6] Metal-containing precursors other than films, such as nanostrands, nanobelts, nanoparticle networks, and nanosheets, have also been used for MOF-VPD.[17,23−25] During the vapor−solid reaction step, the linker exposure time, temperature, and humidity need to be carefully controlled. To date, a variety of MOF thin films have been deposited by the MOF-VPD

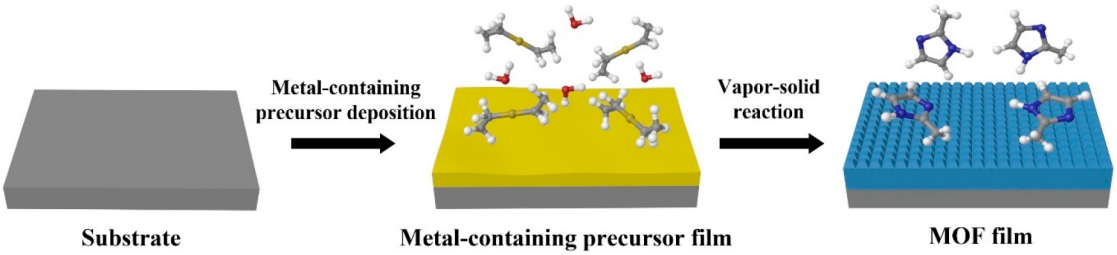

Figure 1. MOF-VPD process consisting of deposition of a metal-containing precursor and a consecutive vapor−solid reaction to form the MOF film.

Table 1. Summary of the MOF-VPD Method for MOF Film Deposition[a]

MOF film	MOF film thickness (nm)	metal-containing precursor	precursor layer thickness (nm)	linker	additional vapor	T (°C)	ref(s)
ZIF-8	30−124	ZnO	3−15	HmIm	N	100−120	1, 22
ZIF-8	17−757	Zn-gel	NA	HmIm	N	150	2
ZIF-8_Cl	85−245	ZnO	5−15	HIm-Cl	DMF	110	4
ZIF-8_Br	79	ZnO	5	HIm-Br	DMF	110	4
ZIF-7	NA	ZnO	5	HbIm	DMF	110	4
ZIF-71	101	ZnO	5	HdcIm	DMF or EtOH	110	4
ZIF-72	63	ZnO	5	HdcIm	N	150	4
MAF-6	90	ZnO	3−10	HeIm	N	110	26
MAF-252	19−109	ZnO	1−11	Hdpt	N	200	27
ZIF-61	NA	ZnO	15	HIm	N	90	1
ZIF-67	NA	$Co(acac)_2$[b]	NA	HmIm	H_2O	95−125	28
ZIF-67	NA	CoO	10	HmIm	N	120	1
$Co_2(bim)_4$	57−750	Co-gel	NA	HbIm	N	190	29
CuBDC	83−200	CuO	15−100	H_2BDC	N or H_2O	200	30
CuCDC	87−190	CuO	15−100	H_2CDC	N or H_2O	200	30
$[Mg_3(HCOO)_6]$	NA	MgO	10−20	FA	DMSO, DMF	100	31
$[Zn_4O(dmcapz)_6]$	NA	ZnO	30	H_2dmcapz	AA and DMF	170	21
$(DMA)_2[Zn_3(bdc)_4]$	NA	ZnO	30	H_2BDC	AA and DMF	240	21

[a]Abbreviations: NA, not available; N, no additional vapor; HIm, 1*H*-imidazole; HmIm, 2-methylimidazole; HIm-Cl, 2-chloroimidazole; HIm-Br, 2-bromoimidazole; HbIm, benzimidazole; HdcIm, 4,5-dichloroimidazole; HeIm, 2-ethylimidazole; Hdpt, 3-(2-pyridyl)-5-(4-pyridyl)-1,2,4-triazole; H_2BDC, 1,4-benzenedicarboxylic acid; H_2CDC, *trans*-1,4-cyclohexanedicarboxylic acid; H_2dmcapz, 3,5-dimethyl-4-carboxypyrazole; DMA, dimethylammonium; DMF, *N*,*N*-dimethylformamide; DMSO, dimethyl sulfoxide; EtOH, ethanol; $Co(acac)_2$, cobalt(II) acetylacetonate; FA, formic acid; AA, acetic acid. [b]Powder form.

method (Table 1). Among them, ZIF-8 has been studied the most. Thus, we use ZIF-8 as a case study to discuss some important aspects of the vapor−solid reactions during MOF-VPD.

ZIF-8 is constructed from Zn^{2+} and 2-methylimidazolate (HmIm) to form a sodalite (SOD) topology.[10] MOF-VPD of a ZIF-8 thin film was first realized by the neutralization reaction between ALD ZnO and HmIm vapor.[1] Compared with the solvothermal conversion of ZnO to ZIF-8,[32] the vapor-phase conversion avoided the dissolution of ZnO and enabled the localized transformation of the ultrathin precursor film (3 nm thick) with high fidelity. To gain further insights into the oxide-to-MOF conversion, Ameloot and co-workers developed a single-chamber MOF-VPD process that allowed in situ ellipsometry monitoring.[22] The temperature gradient between the reactor wall and substrate was found to be critical to ensure adsorption of HmIm on the ZnO surface instead of the reactor walls, analogous to polymer CVD.[33] Time-resolved in situ ellipsometry showed a sigmoidal thickness expansion as a function of HmIm linker exposure time, which represented three MOF-VPD stages: (i) adsorption of the HmIm linker vapor on the ZnO surface and reactive diffusion into the layer; (ii) nucleation of ZIF-8 once a critical linker concentration was reached in the ZnO precursor; and (iii) continued nucleation and growth until a defect-free and uniform ZIF-8 film was formed (Figure 2a,b). Water was shown to facilitate both the vapor-phase ZnO-to-ZIF-8 conversion and the subsequent ripening of the MOF crystallites, resulting in more pronounced crystal facets and rougher films compared with nonhumidified conditions.[22] This behavior was attributed to direct hydroxylation of ZnO and protonation of the linker, which subsequently accelerated the oxide-to-MOF conversion and crystal ripening.[34,35] Because of the low mobility of zinc ions, the ZIF-8 films prepared by vapor deposition displayed an exceptionally smooth surface with a root-mean-square roughness of 4.4 nm, which is lower than that of most ZIF-8 films fabricated by solvothermal synthesis.[22] Through the mechanistic study of the vapor−solid reaction, the optimized deposition conditions (e.g., process temperature, oxide thickness, humidity, and linker exposure time) were identified and successfully translated to 200 mm Si wafer substrates (Figure 2c). Acidic vapors such as formic acid and acetic acid can also facilitate the precursor-to-MOF transformation, as illustrated for the conversion of aluminum nitride by the fumaric acid linker to form Al-MIL-53-Fum.[36]

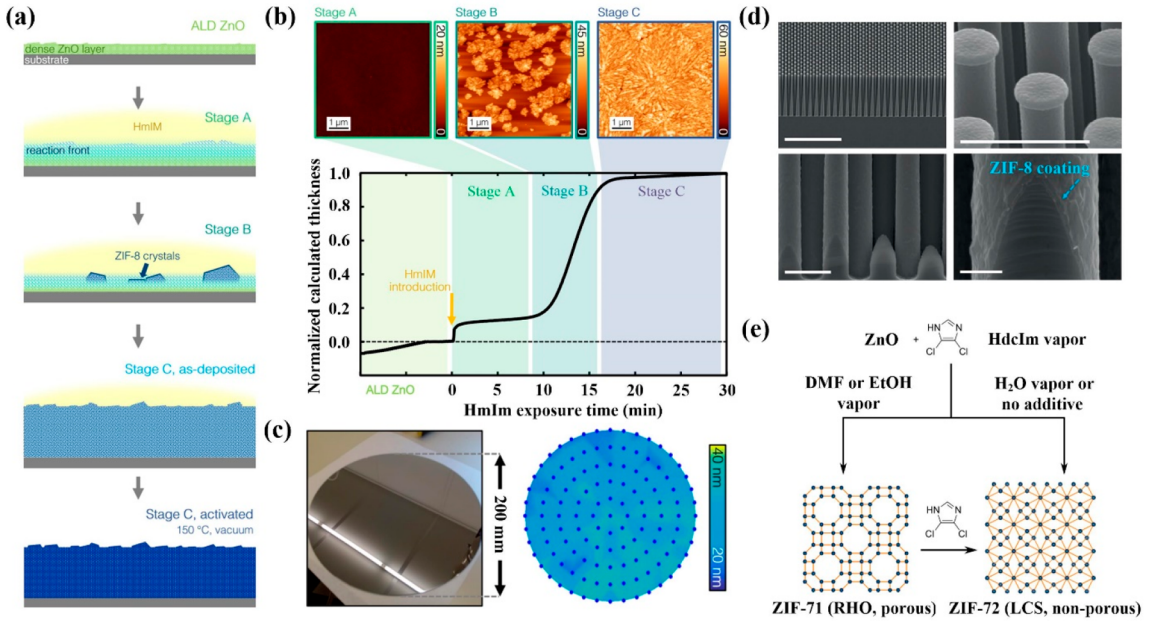

Figure 2. Vapor-phase deposition of MOFs. (a) Schematic illustration of the MOF-VPD growth stages. (b) Time-resolved in situ ellipsometry profiles and atomic force microscopy (AFM) images collected at different growth stages. (c) Photograph of a 200 mm wafer with a MOF-VPD ZIF-8 coating and the corresponding ellipsometry thickness mapping. Reproduced from ref 22. Copyright 2019 American Chemical Society. (d) SEM images of the deposition of a conformal ZIF-8 thin film on high-aspect-ratio pillar arrays. Reproduced with permission from ref 1. Copyright 2015 Nature Publishing Group. (e) Illustration of vapor-template-mediated topology control during the vapor-phase synthesis of ZIF-71 and ZIF-72. Reproduced with permission from ref 4. Copyright 2020 Wiley-VCH.

Thickness control is of high importance for the integration of thin-film materials into miniaturized devices. The transformation of a dense metal-containing precursor layer into a highly porous MOF film causes an expansion of the film thickness, which can be estimated by thickness expansion $= \frac{M_{MOF} \times \rho_{precursor}}{M_{precursor} \times \rho_{MOF}}$, where M_{MOF} and $M_{precursor}$ are the molecular weights of the MOF and the precursor (per mole of metal), respectively, and ρ_{MOF} and $\rho_{precursor}$ are their respective densities. In the case of ZIF-8, a 16.5-fold thickness increase is theoretically expected, considering the molecular weights of 81.4 and 227.6 g mol^{-1} for ZnO and Zn(mIm)$_2$, respectively, and the densities of 5.6 and 0.95 g cm^{-3} for crystalline ZnO and ZIF-8, respectively. In the case of low-density ALD ZnO, the oxide-to-MOF thickness expansion factor was found to be lower (10 instead of 16.5) because of hydroxyl defects in the precursor film.[22] Moreover, when thicker precursor layers are converted, the initially formed MOF layers may limit the diffusion of the linker to the MOF–precursor interface, decreasing the crystallization rate and leading to less thick MOF layers than expected for complete conversion. When thick MOF layers (up to >200 μm) are required, this limitation can be avoided by using a highly porous precursor layer.[25] In addition to control over the film thickness, MOF-VPD also enabled a highly conformal coating, as demonstrated by ZIF-8 deposition on high-aspect-ratio silicon pillar arrays (Figure 2d).

The type of precursor plays an important role in the MOF-VPD process. Ameloot and co-workers found that defective ZnO (i.e., with many hydroxyl defects) showed fast conversion, while highly crystalline and less defective ZnO (high-temperature-annealed or deposited by sputtering) is more difficult to transform.[37] For crystalline precursors, the crystal planes terminating the surface also play a role in determining the ease of the oxide-to-MOF transformation. For example, it was found that ZnO nanorods were transformed more easily into ZIF-8 in the presence of HmIm vapor compared with ZnO nanoparticles. A study of ZnO single crystals found that the conversion to ZIF-8 was highest on the m plane ($10\bar{1}0$). The easy transformation of ZnO nanorods into ZIF-8 is likely explained by the dominance of this crystal plane in the surface termination, in contrast to ZnO nanoparticles, where a significant contribution of the less reactive c plane (0001) is expected.[20]

For both bulk MOF powders and thin films, a key feature is the porosity. Several quantitative porosimetry methods have been developed for MOF films that involve measurement of the adsorbed quantity of probe molecules, such as volumetric Kr physisorption, gravimetric quartz crystal microbalance, and ellipsometric porosimetry.[1,38−40] The conformal MOF-VPD coatings on high-aspect-ratio pillar arrays allowed direct Kr sorption measurements on samples of practical size (e.g., 1 cm^2 of wafer patterned as a pillar array). The Brunauer–Emmett–Teller surface areas of MOF-VPD films, as determined by Kr physisorption, were close to the values reported for powder samples.[1,4,22] Positron annihilation lifetime spectroscopy, which does not require a probe molecule, has recently been used to gain pore size information and perform depth profiling in MOF films.[4,26] A comprehensive discussion of the use of these techniques to understand MOF film porosity has been reported by Ameloot and co-workers.[41]

The landscape of possible polymorphs for some MOFs can pose a challenge for controlling the MOF-VPD synthesis outcome.[42,43] For instance, the direct vapor–solid reaction between ZnO and 4,5-dichloroimidazole (HdcIm) vapor led to the formation of the dense ZIF-72 phase (LCS topology) instead of the porous ZIF-71 phase (RHO topology).[4] Ameloot and co-workers employed time-resolved synchrotron

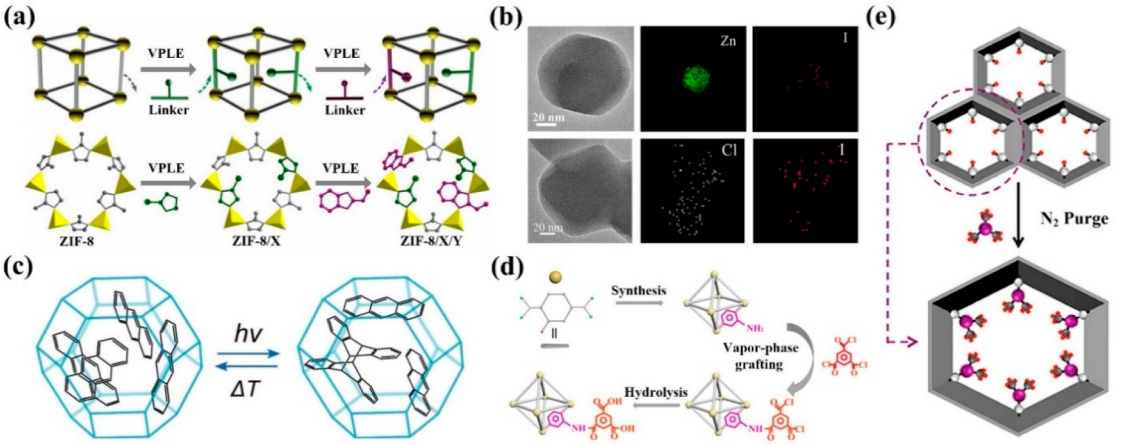

Figure 3. Vapor-phase postsynthetic functionalization of MOFs. (a) Scheme of multistep VPLE of MOFs. (b) TEM and EDS mapping images of ZIF-8/I and ZIF-8/I/Cl. From ref 3. CC BY-NC 4.0. (c) Photodimerization in anthracene-loaded ZIF-8. Reproduced with permission from ref 57. Copyright 2019 Wiley-VCH. (d) Schematic illustration of postsynthetic functionalization of MOFs by vapor-phase grafting. Reproduced from ref 58. Copyright 2021 American Chemical Society. (e) Schematic illustration of vapor-phase metalation by ALD in a MOF. Reproduced from ref 59. Copyright 2013 American Chemical Society.

small-angle X-ray scattering (SAXS) to monitor the oxide-to-MOF conversion in situ.[4] The study revealed the transition from the metastable porous phase (ZIF-71) into the more thermodynamically stable dense phase (ZIF-72), following Ostwald's rule of stages.[44] Moreover, it was found that introducing a template vapor (DMF or EtOH) could prohibit this phase transition (Figure 2e). The templating effect was attributed to hydrogen bonding between the template and linker, stabilizing the porous structure. Template-mediated polymorphism control has also been demonstrated for other members of the ZIF family and α-magnesium formate $[Mg_3(HCOO)_6]$.[4,31] In contrast, the formation of ZIF-8 and MAF-6 by MOF-VPD did not require the addition of a template since the linker itself fills the pores during crystallization, possibly due to $CH_3\cdots\pi$ interactions between methyl or ethyl groups and the imidazole ring.[1,26]

Apart from ZIFs, a variety of MOFs have been deposited by MOF-VPD using other precursor layers (Cu, CuO, MgO, etc.) and carboxylate linkers (Table 1). Furthermore, the introduction of additional components (e.g., metal and polymer) into the resulting MOFs could be achieved through linker-vapor-assisted conversion of functionalized metal-containing precursors.[45] For example, zinc hydroxide nanostrands were mixed with sulfonate-ion-containing heparin for fabrication of a sulfonated ZIF-8 membrane by exposure to HmIm vapor.[46] The sulfonated nanochannels in the ZIF-8 membrane provided fast and selective transport paths for Li^+ because of size sieving, electrostatic interaction, and ionic rectification. Orientation control is another important topic for thin-film deposition. Although MOF-VPD films are typically randomly oriented, the CuBDC and CuCDC films obtained this way showed a preferred [100] orientation.[30] In addition, a [001]-oriented ZIF-67 film was obtained by decreasing the growth rate. The mechanism governing the formation of such a preferred orientation is still unclear at this point.[28]

Besides the two-step MOF-VPD process, molecular layer deposition (MLD) has been applied to deposit MOF films through alternation of the deposition of volatile metal-containing precursors and linker vapors.[47,48] During each deposition step, a self-saturating reaction takes place between the reactive vapor and the surface. In most cases, the deposited film is amorphous but can be crystallized through a subsequent treatment. In the first report, Salmi and co-workers prepared MOF-5 thin films by MLD using zinc acetate and 1,4-benzenedicarboxylic acid (H_2BDC), followed by crystallization under humid conditions.[49] Nilsen and co-workers reported that MLD of $ZrCl_4$ and H_2BDC produced amorphous films with a growth rate of 6–7 Å $cycle^{-1}$.[50] The growth rate was demonstrated by an in situ quartz crystal microbalance (QCM) study. Subsequent exposure of these films to acetic acid vapor resulted in the formation of crystalline UiO-66 films. Since the film morphology and roughness change during postdeposition crystallization, the advantage of thickness control that MLD offers in principle is partially offset. In other cases, crystalline as-deposited films could be achieved directly, though their porosity has not been investigated in detail.[51,52] To fully realize the potential of MOF-MLD, further investigations are required with regard to precursor selection, the effect of additives, and the processing parameters necessary to realize crystalline as-deposited films.

VAPOR-PHASE POSTSYNTHETIC FUNCTIONALIZATION OF MOFS

Postsynthetic functionalization (PSF) is an efficient approach to adjust the physicochemical properties of MOFs. PSF is often implemented by functionalization of the linkers, loading of guest molecules, or substitution of the original building blocks by other metal ions or linkers.[53−55] Vapor-phase PSF of MOFs can be realized through the vapor−solid reactions between MOFs and vaporized metal-containing precursors, linkers, and reagents.[3] This approach eliminates potential solubility issues and enables the fast diffusion of reactants and guests as well as a high loading or degree of exchange.

Ameloot and Li have indicated that there are three steps in a typical vapor-phase linker exchange (VPLE) process: (i) adsorption of the incoming linker; (ii) exchange of protons between the adsorbed linker and the parent linker; and (iii) desorption of the parent linker.[3,8,56] To realize efficient VPLE, three criteria should be considered: (i) the incoming linker should be able to protonate the linker in the framework; (ii) the protonated forms of both linkers should be sufficiently

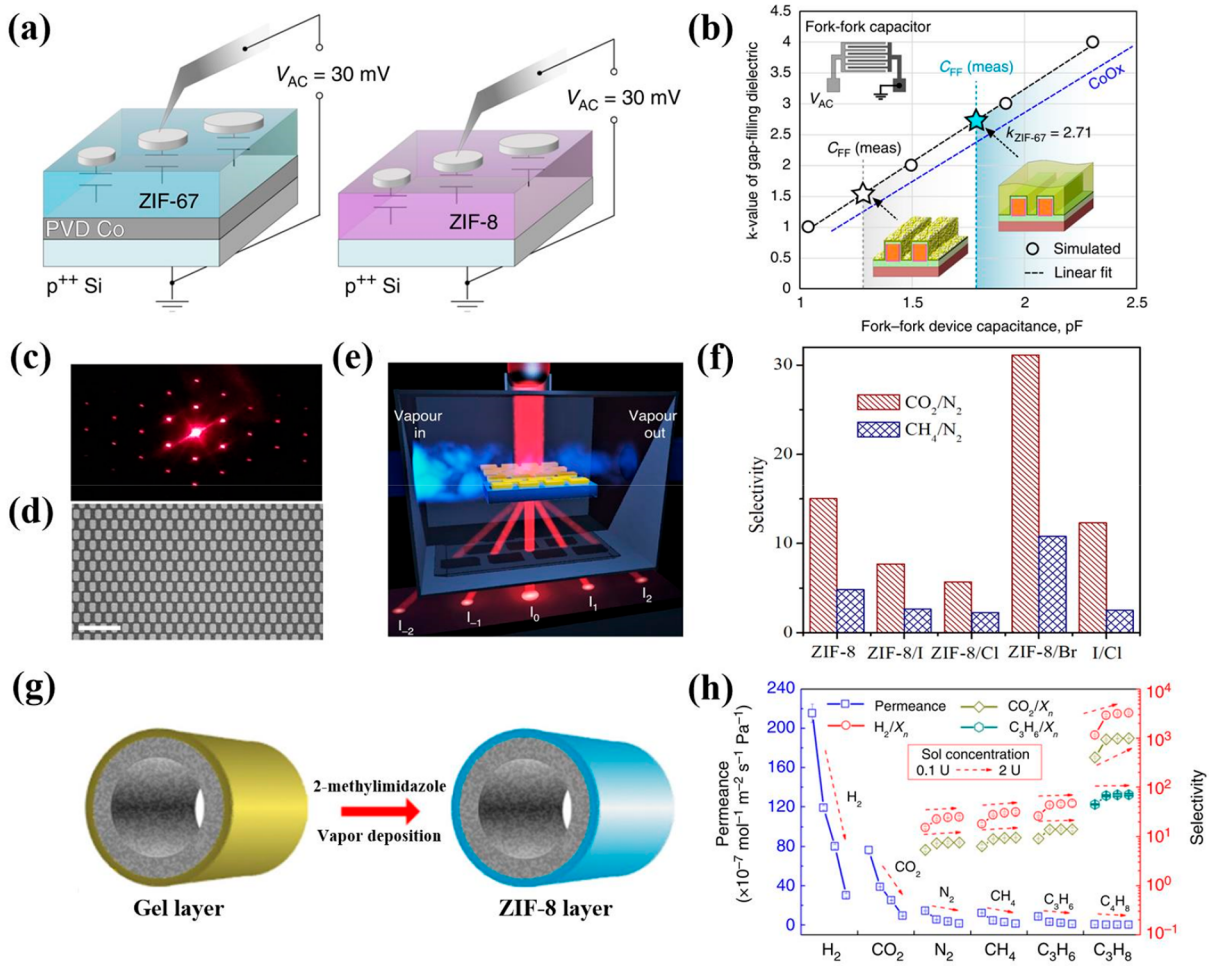

Figure 4. Applications of MOF-VPP. (a) Schematic illustration of *k*-value measurements for MOF-VPD ZIF-8 and ZIF-67 films. (b) Determination of the *k* value for the gap-filling ZIF-67 material. From ref 39. CC BY 4.0. (c) Diffraction pattern through illumination of a ZIF-71 pattern on quartz with a red laser pointer. (d) Optical microscopy image of the ZIF-71 pattern used as a diffraction grating. Scale bar: 100 μm. (e) Schematic illustration of the evaluation of ZIF-71 patterns used as diffraction grating vapor sensors. Reproduced with permission from ref 40. Copyright 2020 the authors of ref 40, under exclusive license to Springer Nature. (f) CO_2/N_2 and CH_4/N_2 adsorption selectivities of ZIF-8 and linker-exchanged ZIFs calculated by Henry's law. From ref 3. CC BY-NC 4.0. (g) Fabrication of ZIF-8 membrane by gel vapor deposition. (h) Gas transport performances of the MOF-VPD ZIF-8 membrane. From ref 2. CC BY 4.0.

volatile; and (iii) the incoming linker should coordinate the metal cations while preserving the parent topology. In the case of VPLE of ZIF-8 by 2-carboxaldehyde imidazole (CHO-HIm), the HmIm linker was substituted by CHO-HIm to form a mixed-linker MOF.[56] Different from the traditional solvent-assisted linker exchange, VPLE could break the diffusion limitations during the exchange process, resulting in an identical fraction (84 ± 6%) of CHO-HIm incorporated into ZIF-8 with different particle sizes. Other imidazole linkers, including 2-nitroimidazole (NO_2-HIm), benzimidazole (HbIm), and HdcIm, could also be incorporated by VPLE. Moreover, multistage VPLE can be carried out to achieve "multivariate" MOFs with multiple linkers. For instance, ZIF-8/I/Cl can be realized by a tandem VPLE, i.e., exposure of ZIF-8 to 4-iodoimidazole (I-HIm) and 2-chloromethylbenzimidazole (HClbIm) vapors sequentially (Figure 3a,b).[3] Neither loss of crystallinity nor changes in morphology were observed after the exchange process. Furthermore, functionalization of MOFs can improve the interface compatibility between the modified particles and polymers. For example, more polar ZIF-8/I and ZIF-8/Br nanoparticles obtained by VPLE could be homogeneously distributed in polysulfone, whereas the ZIF-8/polysulfone composite suffered from filler agglomeration and interfacial defects.

Vapor-phase guest loading can prevent solubility issues of guest molecules and competition from solvent molecules, leading to high loadings. Ameloot and co-workers achieved a loading of up to four anthracene (ANT) molecules per ZIF-8 cage through sublimation.[57] The ANT molecules were organized as two pairs in each cage, giving rise to yellow excimer emission. Upon UV irradiation, two ANT molecules photodimerize, resulting in one nonfluorescent ANT photodimer and two randomly distributed ANT molecules (Figure 3c). As a result, the emission color changes from yellow to purple because of the replacement of excimer emission by monomer emission. This solid-state photoswitching allowed the development of photopatternable, erasable, and rewritable paper with potential applications in product authentication and secure communication.

Covalent postsynthetic modifications on the linkers are often employed to tailor the physicochemical properties of MOFs.[53] Compared with solvent-based grafting methods, vapor-phase

linker grafting can lead to higher yields of introduced functional groups. For example, amino-functionalized IRMOF-3 was grafted with vaporized salicylaldehyde in 99% yield without loss of crystallinity.[60] Li and co-workers reported the vapor-phase grafting of NH_2-UiO-66 by exposure to vaporized trimesoyl chloride based on the Schotten−Baumann reaction (Figure 3d). Through simple immersion in water, the MOF grafted with acyl chloride groups was transformed into a carboxylated material with high porosity and improved fluoride removal performance.[58] Vapor-phase metalation can be conducted in MOFs by ALD, which can deposit metals or metal oxides on the uncoordinated nodes of MOFs with high density (Figure 3e).[59] This approach breaks the limitation of metal-containing precursor solubility and shows potential in catalyst preparation.[18,61]

APPLICATIONS

Benefiting from the merits of MOF-VPD methods (e.g., high uniformity, low defects, solvent-free, and conformal coating), MOF films with improved performance can be fabricated on various substrates, for example, on porous alumina and polymer supports for membrane separations as well as on nonporous wafers for low-*k* dielectrics. Moreover, the physicochemical properties of MOFs can be tuned by vapor-phase functionalization toward specific applications.[17,62]

Because of their low dielectric constant, MOFs have become a promising class of dielectric materials.[63] The integration of MOFs as low-*k* dielectrics in interconnects is a challenging task. Ameloot and co-workers adopted the MOF-VPD approach to deposit MOFs as gap-filling dielectrics between metal interconnect lines. As shown in Figure 4a, ZIF-8 and ZIF-67 films were deposited on conductive substrates by the vapor-phase conversion of ALD ZnO and native CoO_x films, respectively.[39] The *k* values determined from thin-film parallel-plate capacitor measurements at 100 kHz were 2.23 ± 0.11 and 2.39 ± 0.18 for ZIF-8 and ZIF-67 films, respectively. The higher *k* value of the Co-based ZIF-67 was attributed to the more polar Co−N bonds in contrast with Zn−N. Thanks to the expansion during the precursor-to-MOF conversion, VPD ZIF-67 could successfully fill the gaps in 45 nm pitch fork−fork capacitors. Through 2D finite-element capacitance simulations, the effective *k* value of the gap-filling ZIF-67 was calculated to be 2.71 at 100 kHz, slightly exceeding the value determined for blanket ZIF-67 films (Figure 4b).

Apart from thin film deposition, lithographic patterning is another fundamental step to integrate MOFs into miniaturized devices. Direct resist-free lithography of MOFs is desirable to minimize the number of process steps and possible contamination sources. Ameloot and co-workers found that halogenated ZIF films fabricated by MOF-VPD exhibited a solubility switch after X-ray and electron-beam exposure.[40] This direct patterning capability was used to fabricate photonic gas sensors by patterning MOF films into highly regular optical diffraction gratings. Because of the spatial periodicity in the refractive index, the patterned ZIF-71 film on a transparent substrate could be used as a diffraction phase grating for light in the visible range (Figure 4c,d). When guest molecules adsorbed in the pores, the phase difference resulting from the MOF pattern increased together with the refractive index of the MOF layer. Therefore, gas/vapor sensing could be realized by monitoring the intensity changes of the first-order diffraction spots, which was illustrated for methanol vapor sensing using a 200 nm thick ZIF-71 diffraction grating (Figure 4e).

Adsorptive CO_2/N_2 and CH_4/N_2 separations are significant challenges because of their similar kinetic diameters. Li and co-workers used the VPLE strategy to introduce halogen functional groups in ZIF frameworks.[3] The resulting ZIF-8/Br materials displayed an excellent CO_2/N_2 selectivity of 31.1, approximately twice as high as that of ZIF-8 (15.0) (Figure 4f). In addition to carbon capture, the separation of CH_4 and N_2 in natural gas/biogas purification is vital for chemical and energy-related industries. The prepared ZIF-8/Br showed a remarkable CH_4/N_2 selectivity of 10.8, which is 2−6 times higher than those typically reported for porous carbons, zeolites, and MOFs. Besides gas adsorption, MOF-VPD has been used to deposit ZIF-8 on solid-phase microextraction fibers, which was able to combine gas chromatography and flame ionization detection for various target analytes such as polycyclic aromatic hydrocarbons and personal care products.[64]

MOF-VPD can produce ultrathin MOF molecular sieving membranes with high permeance and selectivity and minimal pinholes and defects. Li and co-workers prepared ultrathin ZIF-8 gas separation membranes by combining sol−gel coating and solvent-free vapor conversion (Figure 4g).[2] A Zn-based gel prepared from zinc acetate dihydrate and ethanolamine was coated on hollow polymer fibers as a versatile metal-containing precursor. In the subsequent exposure to vaporized HmIm, a continuous ZIF-8 membrane was produced. The thickness of these membranes could be precisely controlled via the coating time and sol concentration (e.g., 17 nm of ZIF-8 for a coating time of 2 s). This scalable gel vapor deposition method was already applied to prepare a MOF hollow fiber membrane module (30 polysulfone hollow fibers, membrane area of 340 cm^2). As shown in Figure 4h, the ZIF-8 membranes displayed a high H_2 permeance of 119.0 × 10^{-7} mol m^{-2} s^{-1} Pa^{-1} and excellent gas selectivities of 22.4, 27.3, 43.1, and 2894 for H_2/N_2, H_2/CH_4, H_2/C_3H_6, and H_2/C_3H_8, respectively, together with outstanding stability over 274 h. Tsapatsis and co-workers prepared a continuous ZIF-8 membrane by all-vapor-phase processing based on ALD of ZnO onto porous alumina supports followed by HmIm vapor treatment. The resulting membranes showed a C_3H_6 permeance of 368 × 10^{-10} mol m^{-2} s^{-1} Pa^{-1} and a high C_3H_6/C_3H_8 selectivity of 152.[5] Moreover, VPLE can enhance the gas separation performance of MOF membranes. Exchanging the HmIm linker in ZIF-8 membranes with more bulky 2-aminobenzimidazole (2abIm) reduces the effective pore size and results in a clear selectivity improvement toward smaller gas molecules.[65] In addition to VPLE, vapor treatment using volatile metal−organic compounds has been shown to be an effective route to tune MOF membranes. Tsapatsis and co-workers treated ZIF-8 membranes with manganese(II) acetylacetonate ($Mn(acac)_2$) vapor, resulting in an increase in C_3H_6/C_3H_8 selectivity from 31 to 210.[66]

CONCLUSIONS AND OUTLOOK

In this Account, we have summarized our recent advances in vapor-phase deposition and postsynthetic functionalization of MOFs. Through the combination of well-established vapor-phase deposition and the vapor−solid reaction, MOF-VPD realizes the controllable deposition of MOF thin films on various substrates as well as the conformal coating of intricate morphologies, such as nanoarrays, nanosheets, and nanofibers. In addition, we have presented four vapor-phase PSF strategies

for tuning the MOF properties or introducing new functionalities: linker exchange, guest loading, linker grafting, and metalation. These strategies will likely facilitate the application of MOFs in various fields, including low-*k* dielectrics, chemical sensing, adsorption, membrane separation, etc.

While the developments of MOF-VPP outlined in this Account are highly encouraging, substantial challenges still need to be addressed. First, a further understanding of the MOF-VPP mechanisms is desired, as such insights will be critical in developing novel processes and large-scale production. Monitoring MOF-VPP by in situ techniques (e.g., X-ray scattering, ellipsometry, infrared/Raman spectroscopy, and electron microscopy) will greatly facilitate the understanding of nucleation, on-surface precursor mobility, reaction pathways, crystallographic orientation, polymorphism control, etc. Second, further improving the MOF film quality (e.g., grain boundaries, surface roughness, and crystallographic orientation) is highly important, especially for applications that require defect-free films/membranes. MOF-VPD films still show high roughness compared with inorganic thin films deposited by established vapor-phase methods such as ALD. Moreover, oriented thin films are desired in several scenarios, such as solid-state electrolytes, memristors, and field-effect transistors. Through fine-tuning of the deposition process to control the nucleation and growth kinetics, oriented and low-roughness films may be obtained. Third, compared with the huge number of available MOF structures, the number of films that can be deposited by MOF-VPD is still limited. The current MOF-VPD research mostly focuses on ZIFs because of the relatively high volatility of imidazole linkers, the reactivity of metal-containing precursors, and the fact that they form more readily under mild conditions compared with MOFs based on higher-valence metal ions or in which the framework nodes are metal ion clusters instead of individual ions. The extension to other MOFs requires the careful selection of precursors (e.g., a relatively high vapor pressure and sufficient thermal stability) and control over the deposition process (e.g., temperature, pressure, and humidity). As in a liquid-phase synthesis, the topological diversity of MOFs can pose a challenge for controlling the synthesis outcome within a landscape of possible polymorphs. For some cases, this challenge has been shown to be addressed through introducing a vapor-phase "structure-directing agent".[4,31] In addition to linker exchange, it will be interesting to see whether vapor-phase cation substitution can be realized.

Patterning is another important step for the integration of MOFs into miniaturized devices. Though few cases of MOF patterning have been demonstrated using well-established lithographic processes, not much is known about the influence of the photoresist and etch chemistry on MOF properties such as crystallinity, surface area, pore accessibility, and defectivity. We recently demonstrated resist-free lithography of MOFs by X-ray or electron-beam lithography, which avoids resist contamination and minimizes the number of processing steps.[40] However, since such a process is limited to halogenated ZIFs for now, further research to extend the scope is needed. Also, the effect of MOF layers on subsequent processing steps in microfabrication, and vice versa, should be explored. Apart from the low-*k* dielectrics and membrane separations discussed here, further development will facilitate the application of MOF-VPP in chemical sensors, memory resistors for data storage, photodetectors, light-emitting diodes, etc. Through the further efforts on the aspects discussed above, we foresee a bright future for MOF-VPP methods.

AUTHOR INFORMATION

Corresponding Authors

Min Tu − *2020 X-Lab and State Key Laboratory of Transducer Technology, Shanghai Institute of Microsystem and Information Technology, Chinese Academy of Sciences, Shanghai 200050, China;* orcid.org/0000-0003-4751-3877; Email: min.tu@mail.sim.ac.cn

Rob Ameloot − *Centre for Membrane Separations, Adsorption, Catalysis, and Spectroscopy, KU Leuven - University of Leuven, 3001 Leuven, Belgium;* orcid.org/0000-0003-3178-5480; Email: rob.ameloot@kuleuven.be

Wanbin Li − *Guangdong Key Laboratory of Environmental Pollution and Health, School of Environment, Jinan University, Guangzhou 511443, China;* orcid.org/0000-0003-2460-168X; Email: gandeylin@126.com

Author

Pengcheng Su − *Guangdong Key Laboratory of Environmental Pollution and Health, School of Environment, Jinan University, Guangzhou 511443, China;* orcid.org/0000-0002-0146-3475

Complete contact information is available at: https://pubs.acs.org/10.1021/acs.accounts.1c00600

Notes

The authors declare no competing financial interest.

Biographies

Pengcheng Su obtained his Ph.D. at the Zhejiang University of Technology in China in 2020 and then conducted his postdoctoral research at Jinan University in China, mentored by Prof. Wanbin Li. His current research interests mainly focus on the rational design and preparation of MOF materials and membranes with application in molecular sieving.

Min Tu obtained his Ph.D. in 2015 at Ruhr University Bochum in Germany under the supervision of Prof. Roland A. Fischer (now at TU Munich). Supported by a Marie Skłodowska-Curie Actions Fellowship, he worked as a postdoctoral fellow at KU Leuven in Belgium, mentored by Prof. Rob Ameloot. Currently he is an independent group leader at Shanghai Institute of Microsystem and Information Technology, Chinese Academy of Sciences. His research interests focus on the integration of nanoporous materials into miniaturized devices using micro- and nanofabrication technologies.

Rob Ameloot obtained his Ph.D. at KU Leuven and was a Fulbright postdoctoral fellow at UC Berkeley in the United States. Currently, he is a tenured professor at KU Leuven. He was awarded ERC Starting and Proof-of-Concept Grants to bring microporous materials from the chemistry lab into the microelectronics lab. In general, he is passionate about pushing the envelope in porous materials and their applications, with a healthy disregard for traditional subject boundaries.

Wanbin Li received his Ph.D. from Zhejiang University of Technology in 2016 and since then has worked at Jinan University as an associate professor. His research interests focus on developing novel membranes and other functional materials based on MOFs, 2D materials, polymers, etc. and controlling the transport processes and adsorption properties for gas separation and water treatment.

■ ACKNOWLEDGMENTS

M.T. acknowledges financial support by the National Key R&D Program of China (2021YFB3200800) and the Shanghai Pujiang Program (21PJ1415200). W.L. acknowledges funding from the National Natural Science Foundation of China (Grant 22178143) and the Guangdong Basic and Applied Basic Research Foundation (Grants 2020B1515120036 and 2021A1515010187). R.A. acknowledges funding from the European Research Council (ERC) under the European Union's Horizon 2020 Research and Innovation Programme (Grant Agreement 716472, acronym: VAPORE). R.A. acknowledges funding from the Research Foundation Flanders (FWO Vlaanderen) through Projects G85720N and G0E6319N and from KU Leuven through Project C14/20/085.

■ REFERENCES

(1) Stassen, I.; Styles, M.; Grenci, G.; Van Gorp, H.; Vanderlinden, W.; De Feyter, S.; Falcaro, P.; De Vos, D.; Vereecken, P.; Ameloot, R. Chemical Vapour Deposition of Zeolitic Imidazolate Framework Thin Films. *Nat. Mater.* **2016**, *15*, 304−310.

(2) Li, W.; Su, P.; Li, Z.; Xu, Z.; Wang, F.; Ou, H.; Zhang, J.; Zhang, G.; Zeng, E. Ultrathin Metal−Organic Framework Membrane Production by Gel−Vapour Deposition. *Nat. Commun.* **2017**, *8*, No. 406.

(3) Wu, W.; Su, J.; Jia, M.; Li, Z.; Liu, G.; Li, W. Vapor-Phase Linker Exchange of Metal-Organic Frameworks. *Sci. Adv.* **2020**, *6*, No. eaax7270.

(4) Tu, M.; Kravchenko, D. E.; Xia, B.; Rubio-Giménez, V.; Wauteraerts, N.; Verbeke, R.; Vankelecom, I.; Stassin, T.; Egger, W.; Dickmann, M.; Amenitsch, H.; Ameloot, R. Template-Mediated Control over Polymorphism in the Vapor-Assisted Formation of Zeolitic Imidazolate Framework Powders and Films. *Angew. Chem., Int. Ed.* **2021**, *60*, 7553−7558.

(5) Ma, X.; Kumar, P.; Mittal, N.; Khlyustova, A.; Daoutidis, P.; Mkhoyan, K. A.; Tsapatsis, M. Zeolitic Imidazolate Framework Membranes Made by Ligand-Induced Permselectivation. *Science* **2018**, *361*, 1008−1011.

(6) Van Bui, H.; Grillo, F.; van Ommen, J. R. Atomic and Molecular Layer Deposition: Off the Beaten Track. *Chem. Commun.* **2017**, *53*, 45−71.

(7) Li, W.; Zhang, Y.; Zhang, C.; Meng, Q.; Xu, Z.; Su, P.; Li, Q.; Shen, C.; Fan, Z.; Qin, L.; Zhang, G. Transformation of Metal-Organic Frameworks for Molecular Sieving Membranes. *Nat. Commun.* **2016**, *7*, 11315.

(8) Mandal, S.; Natarajan, S.; Mani, P.; Pankajakshan, A. Post-Synthetic Modification of Metal−Organic Frameworks Toward Applications. *Adv. Funct. Mater.* **2021**, *31*, 2006291.

(9) Jia, M.; Mai, L.; Li, Z.; Li, W. Air-Thermal Processing of Hierarchically Porous Metal−Organic Frameworks. *Nanoscale* **2020**, *12*, 14171−14179.

(10) Park, K. S.; Ni, Z.; Cote, A. P.; Choi, J. Y.; Huang, R.; Uribe-Romo, F. J.; Chae, H. K.; O'Keeffe, M.; Yaghi, O. M. Exceptional Chemical and Thermal Stability of Zeolitic Imidazolate Frameworks. *Proc. Natl. Acad. Sci. U. S. A.* **2006**, *103*, 10186−10191.

(11) Li, W. Metal−Organic Framework Membranes: Production, Modification, and Applications. *Prog. Mater. Sci.* **2019**, *100*, 21−63.

(12) Pichon, A.; Lazuen-Garay, A.; James, S. L. Solvent-Free Synthesis of a Microporous Metal−Organic Framework. *CrystEngComm* **2006**, *8*, 211−214.

(13) Beldon, P. J.; Fábián, L.; Stein, R. S.; Thirumurugan, A.; Cheetham, A. K.; Friščić, T. Rapid Room-Temperature Synthesis of Zeolitic Imidazolate Frameworks by Using Mechanochemistry. *Angew. Chem., Int. Ed.* **2010**, *49*, 9640−9643.

(14) Chen, Y.; Li, S.; Pei, X.; Zhou, J.; Feng, X.; Zhang, S.; Cheng, Y.; Li, H.; Han, R.; Wang, B. A Solvent-Free Hot-Pressing Method for Preparing Metal−Organic-Framework Coatings. *Angew. Chem., Int. Ed.* **2016**, *55*, 3419−3423.

(15) Stassen, I.; Campagnol, N.; Fransaer, J.; Vereecken, P.; De Vos, D.; Ameloot, R. Solvent-Free Synthesis of Supported ZIF-8 Films and Patterns Through Transformation of Deposited Zinc Oxide Precursors. *CrystEngComm* **2013**, *15*, 9308−9311.

(16) Li, W.; Wu, W.; Li, Z.; Shi, J.; Xia, Y. Sol−Gel Asynchronous Crystallization of Ultra-Selective Metal−Organic Framework Membranes for Gas Separation. *J. Mater. Chem. A* **2018**, *6*, 16333−16340.

(17) Stassen, I.; De Vos, D.; Ameloot, R. Vapor-Phase Deposition and Modification of Metal-Organic Frameworks: State-of-the-Art and Future Directions. *Chem. - Eur. J.* **2016**, *22*, 14452−14460.

(18) Islamoglu, T.; Goswami, S.; Li, Z.; Howarth, A. J.; Farha, O. K.; Hupp, J. T. Postsynthetic Tuning of Metal−Organic Frameworks for Targeted Applications. *Acc. Chem. Res.* **2017**, *50*, 805−813.

(19) Lausund, K. B.; Olsen, M. S.; Hansen, P. A.; Valen, H.; Nilsen, O. MOF Thin Films with Bi-Aromatic Linkers Grown by Molecular Layer Deposition. *J. Mater. Chem. A* **2020**, *8*, 2539−2548.

(20) Tanaka, S.; Sakamoto, K.; Inada, H.; Kawata, M.; Takasaki, G.; Imawaka, K. Vapor-Phase Synthesis of ZIF-8 MOF Thick Film by Conversion of ZnO Nanorod Array. *Langmuir* **2018**, *34*, 7028−7033.

(21) Medishetty, R.; Zhang, Z.; Sadlo, A.; Cwik, S.; Peeters, D.; Henke, S.; Mangayarkarasi, N.; Devi, A. Fabrication of Zinc-Dicarboxylate- and Zinc-Pyrazolate-Carboxylate-Framework Thin Films through Vapour−Solid Deposition. *Dalton Trans.* **2018**, *47*, 14179−14183.

(22) Cruz, A. J.; Stassen, I.; Krishtab, M.; Marcoen, K.; Stassin, T.; Rodríguez-Hermida, S.; Teyssandier, J.; Pletincx, S.; Verbeke, R.; Rubio-Giménez, V.; Tatay, S.; Martí-Gastaldo, C.; Meersschaut, J.; Vereecken, P. M.; De Feyter, S.; Hauffman, T.; Ameloot, R. Integrated Cleanroom Process for the Vapor-Phase Deposition of Large-Area Zeolitic Imidazolate Framework Thin Films. *Chem. Mater.* **2019**, *31*, 9462−9471.

(23) Young, C.; Wang, J.; Kim, J.; Sugahara, Y.; Henzie, J.; Yamauchi, Y. Controlled Chemical Vapor Deposition for Synthesis of Nanowire Arrays of Metal−Organic Frameworks and Their Thermal Conversion to Carbon/Metal Oxide Hybrid Materials. *Chem. Mater.* **2018**, *30*, 3379−3386.

(24) Liu, T.; Li, P.; Yao, N.; Kong, T.; Cheng, G.; Chen, S.; Luo, W. Self-Sacrificial Template-Directed Vapor-Phase Growth of MOF Assemblies and Surface Vulcanization for Efficient Water Splitting. *Adv. Mater.* **2019**, *31*, 1806672.

(25) Bo, R.; Taheri, M.; Liu, B.; Ricco, R.; Chen, H.; Amenitsch, H.; Fusco, Z.; Tsuzuki, T.; Yu, G.; Ameloot, R.; Falcaro, P.; Tricoli, A. Hierarchical Metal-Organic Framework Films with Controllable Meso/Macroporosity. *Adv. Sci.* **2020**, *7*, 2002368.

(26) Stassin, T.; Stassen, I.; Marreiros, J.; Cruz, A. J.; Verbeke, R.; Tu, M.; Reinsch, H.; Dickmann, M.; Egger, W.; Vankelecom, I. F. J.; De Vos, D. E.; Ameloot, R. Solvent-Free Powder Synthesis and MOF-CVD Thin Films of the Large-Pore Metal−Organic Framework MAF-6. *Chem. Mater.* **2020**, *32*, 1784−1793.

(27) Stassin, T.; Stassen, I.; Wauteraerts, N.; Cruz, A. J.; Kräuter, M.; Coclite, A. M.; De Vos, D.; Ameloot, R. Solvent-Free Powder Synthesis and Thin Film Chemical Vapor Deposition of a Zinc Bipyridyl-Triazolate Framework. *Eur. J. Inorg. Chem.* **2020**, *2020*, 71−74.

(28) Huang, J.; Saito, N.; Cai, Y.; Wan, Y.; Cheng, C.; Li, M.; Shi, J.; Tamada, K.; Tung, V. C.; Li, S.; Li, L. Steam-Assisted Chemical Vapor Deposition of Zeolitic Imidazolate Framework. *ACS Mater. Lett.* **2020**, *2*, 485−491.

(29) Nian, P.; Liu, H.; Zhang, X. Bottom-Up Fabrication of Two-Dimensional Co-Based Zeolitic Imidazolate Framework Tubular Membranes Consisting of Nanosheets by Vapor Phase Transformation of Co-Based Gel for H_2/CO_2 Separation. *J. Membr. Sci.* **2019**, *573*, 200−209.

(30) Stassin, T.; Rodríguez-Hermida, S.; Schrode, B.; Cruz, A. J.; Carraro, F.; Kravchenko, D.; Creemers, V.; Stassen, I.; Hauffman, T.; De Vos, D.; Falcaro, P.; Resel, R.; Ameloot, R. Vapour-Phase

Deposition of Oriented Copper Dicarboxylate Metal−Organic Framework Thin Films. *Chem. Commun.* **2019**, *55*, 10056−10059.
(31) Kravchenko, D. E.; Cruz, A. J.; Rodríguez-Hermida, S.; Wauteraerts, N.; Hauffman, T.; Ameloot, R. Templated Solvent-Free Powder Synthesis and MOF-CVD Films of the Ultra-microporous Metal−Organic Framework α-Magnesium Formate. *Chem. Mater.* **2020**, *32*, 10469−10475.
(32) Khaletskaya, K.; Turner, S.; Tu, M.; Wannapaiboon, S.; Schneemann, A.; Meyer, R.; Ludwig, A.; Van Tendeloo, G.; Fischer, R. A. Self-Directed Localization of ZIF-8 Thin Film Formation by Conversion of ZnO Nanolayers. *Adv. Funct. Mater.* **2014**, *24*, 4804−4811.
(33) Coclite, A. M.; Howden, R. M.; Borrelli, D. C.; Petruczok, C. D.; Yang, R.; Yagüe, J. L.; Ugur, A.; Chen, N.; Lee, S.; Jo, W. J.; Liu, A.; Wang, X.; Gleason, K. K. 25th Anniversary Article: CVD Polymers: A New Paradigm for Surface Modifi Cation and Device Fabrication. *Adv. Mater.* **2013**, *25*, 5392−5423.
(34) Shi, Q.; Chen, Z.; Song, Z.; Li, J.; Dong, J. Synthesis of ZIF-8 and ZIF-67 by Steam-Assisted Conversion and an Investigation of Their Tribological Behaviors. *Angew. Chem., Int. Ed.* **2011**, *50*, 672−675.
(35) Kwon, H. T.; Jeong, H. K.; Lee, A. S.; An, H. S.; Lee, T.; Jang, E.; Lee, J. S.; Choi, J. Defect-Induced Ripening of Zeolitic-Imidazolate Framework ZIF-8 and Its Implication to Vapor-Phase Membrane Synthesis. *Chem. Commun.* **2016**, *52*, 11669−11672.
(36) Stassin, T.; Waitschat, S.; Heidenreich, N.; Reinsch, H.; Pluschkell, F.; Kravchenko, D.; Marreiros, J.; Stassen, I.; van Dinter, J.; Verbeke, R.; Dickmann, M.; Egger, W.; Vankelecom, I.; De Vos, D.; Ameloot, R.; Stock, N. Aqueous Flow Reactor and Vapour-Assisted Synthesis of Aluminium Dicarboxylate Metal-Organic Frameworks with Tuneable Water Sorption Properties. *Chem. - Eur. J.* **2020**, *26*, 10841−10848.
(37) Cruz, A. J.; Arnauts, G.; Obst, M.; Kravchenko, D. E.; Vereecken, P. M.; De Feyter, S.; Stassen, I.; Hauffman, T.; Ameloot, R. Effect of Different Oxide and Hybrid Precursors on MOF-CVD of ZIF-8 Films. *Dalton Trans.* **2021**, *50*, 6784−6788.
(38) Tu, M.; Wannapaiboon, S.; Khaletskaya, K.; Fischer, R. A. Engineering Zeolitic-Imidazolate Framework (ZIF) Thin Film Devices for Selective Detection of Volatile Organic Compounds. *Adv. Funct. Mater.* **2015**, *25*, 4470−4479.
(39) Krishtab, M.; Stassen, I.; Stassin, T.; Cruz, A. J.; Okudur, O. O.; Armini, S.; Wilson, C.; De Gendt, S.; Ameloot, R. Vapor-Deposited Zeolitic Imidazolate Frameworks as Gap-Filling Ultra-Low-k Dielectrics. *Nat. Commun.* **2019**, *10*, 3729.
(40) Tu, M.; Xia, B.; Kravchenko, D. E.; Tietze, M. L.; Cruz, A. J.; Stassen, I.; Hauffman, T.; Teyssandier, J.; De Feyter, S.; Wang, Z.; Fischer, R. A.; Marmiroli, B.; Amenitsch, H.; Torvisco, A.; Velásquez-Hernández, M. d. J.; Falcaro, P.; Ameloot, R. Direct X-ray and Electron-Beam Lithography of Halogenated Zeolitic Imidazolate Frameworks. *Nat. Mater.* **2021**, *20*, 93−99.
(41) Stassin, T.; Verbeke, R.; Cruz, A. J.; Rodríguez-Hermida, S.; Stassen, I.; Marreiros, J.; Krishtab, M.; Dickmann, M.; Egger, W.; Vankelecom, I. F. J.; Furukawa, S.; De Vos, D.; Grosso, D.; Thommes, M.; Ameloot, R. Porosimetry for Thin Films of Metal−Organic Frameworks: A Comparison of Positron Annihilation Lifetime Spectroscopy and Adsorption-Based Methods. *Adv. Mater.* **2021**, *33*, 2006993.
(42) Cheetham, A. K.; Kieslich, G.; Yeung, H. H. M. Thermodynamic and Kinetic Effects in the Crystallization of Metal−Organic Frameworks. *Acc. Chem. Res.* **2018**, *51*, 659−667.
(43) Karadeniz, B.; Žilić, D.; Huskić, I.; Germann, L. S.; Fidelli, A. M.; Muratović, S.; Lončarić, I.; Etter, M.; Dinnebier, R. E.; Barišić, D.; Cindro, N.; Islamoglu, T.; Farha, O. K.; Friščić, T.; Užarević, K. Controlling the Polymorphism and Topology Transformation in Porphyrinic Zirconium Metal−Organic Frameworks via Mechanochemistry. *J. Am. Chem. Soc.* **2019**, *141*, 19214−19220.
(44) Van Santen, R. A. The Ostwald Step Rule. *J. Phys. Chem.* **1984**, *88*, 5768−5769.
(45) Yi, B.; Zhao, H.; Zhang, Y.; Si, X.; Zhang, G.; An, Y.; Su, L.; Tsung, C.; Chou, L.; Xie, J. A Direct Solvent-Free Conversion Approach to Prepare Mixed-Metal Metal−Organic Frameworks from Doped Metal Oxides. *Chem. Commun.* **2021**, *57*, 3587−3590.
(46) Guo, Y.; Huang, H.; Li, Z.; Wang, X.; Li, P.; Deng, Z.; Peng, X. Sulfonated Sub-Nanochannels in a Robust MOF Membrane: Harvesting Salinity Gradient Power. *ACS Appl. Mater. Interfaces* **2019**, *11*, 35496−35500.
(47) Ahvenniemi, E.; Karppinen, M. Atomic/Molecular Layer Deposition: A Direct Gas-Phase Route to Crystalline Metal−Organic Framework Thin Films. *Chem. Commun.* **2016**, *52*, 1139−1142.
(48) Han, S.; Ciufo, R. A.; Meyerson, M. L.; Keitz, B. K.; Mullins, C. B. Solvent-Free Vacuum Growth of Oriented HKUST-1 Thin Films. *J. Mater. Chem. A* **2019**, *7*, 19396−19406.
(49) Salmi, L. D.; Heikkilä, M. J.; Puukilainen, E.; Sajavaara, T.; Grosso, D.; Ritala, M. Studies on Atomic Layer Deposition of MOF-5 Thin Films. *Microporous Mesoporous Mater.* **2013**, *182*, 147−154.
(50) Lausund, K. B.; Nilsen, O. All-Gas-Phase Synthesis of UiO-66 through Modulated Atomic Layer Deposition. *Nat. Commun.* **2016**, *7*, 13578.
(51) Ahvenniemi, E.; Karppinen, M. In Situ Atomic/Molecular Layer-by-Layer Deposition of Inorganic−Organic Coordination Network Thin Films from Gaseous Precursors. *Chem. Mater.* **2016**, *28*, 6260−6265.
(52) Multia, J.; Heiska, J.; Khayyami, A.; Karppinen, M. Electrochemically Active In Situ Crystalline Lithium-Organic Thin Films by ALD/MLD. *ACS Appl. Mater. Interfaces* **2020**, *12*, 41557−41566.
(53) Cohen, S. M. Postsynthetic Methods for the Functionalization of Metal-Organic Frameworks. *Chem. Rev.* **2012**, *112*, 970−1000.
(54) Liu, L.; Li, L.; Ziebel, M. E.; Harris, T. D. Metal−Diamidobenzoquinone Frameworks via Post-Synthetic Linker Exchange. *J. Am. Chem. Soc.* **2020**, *142*, 4705−4713.
(55) De, S.; Quan, G. C.; Gikonyo, B.; Martineau-Corcos, C.; Bousige, C.; Veyre, L.; Devic, T.; Marichy, C.; Fateeva, A. Vapor-Phase Infiltration inside a Microporous Porphyrinic Metal−Organic Framework for Postsynthesis Modification. *Inorg. Chem.* **2020**, *59*, 10129−10137.
(56) Marreiros, J.; Van Dommelen, L.; Fleury, G.; de Oliveira-Silva, R.; Stassin, T.; Iacomi, P.; Furukawa, S.; Sakellariou, D.; Llewellyn, P. L.; Roeffaers, M.; Ameloot, R. Vapor-Phase Linker Exchange of the Metal−Organic Framework ZIF-8: A Solvent-Free Approach to Post-synthetic Modification. *Angew. Chem., Int. Ed.* **2019**, *58*, 18471−18475.
(57) Tu, M.; Reinsch, H.; Rodríguez-Hermida, S.; Verbeke, R.; Stassin, T.; Egger, W.; Dickmann, M.; Dieu, B.; Hofkens, J.; Vankelecom, I. F. J.; Stock, N.; Ameloot, R. Reversible Optical Writing and Data Storage in an Anthracene-Loaded Metal−Organic Framework. *Angew. Chem., Int. Ed.* **2019**, *58*, 2423−2427.
(58) Rong, S.; Chen, S.; Su, P.; Tang, H.; Jia, M.; Xia, Y.; Li, W. Postsynthetic Modification of Metal−Organic Frameworks by Vapor-Phase Grafting. *Inorg. Chem.* **2021**, *60*, 11745−11749.
(59) Mondloch, J. E.; Bury, W.; Fairen-Jimenez, D.; Kwon, S.; DeMarco, E. J.; Weston, M. H.; Sarjeant, A. A.; Nguyen, S. T.; Stair, P. C.; Snurr, R. Q.; Farha, O. K.; Hupp, J. T. Vapor-Phase Metalation by Atomic Layer Deposition in a Metal−Organic Framework. *J. Am. Chem. Soc.* **2013**, *135*, 10294−10297.
(60) Servalli, M.; Ranocchiari, M.; Van Bokhoven, J. A. Fast and High Yield Post-Synthetic Modification of Metal−Organic Frameworks by Vapor Diffusion. *Chem. Commun.* **2012**, *48*, 1904−1906.
(61) Kim, I. S.; Ahn, S.; Vermeulen, N. A.; Webber, T. E.; Gallington, L. C.; Chapman, K. W.; Penn, R. L.; Hupp, J. T.; Farha, O. K.; Notestein, J. M.; Martinson, A. B. F. The Synthesis Science of Targeted Vapor-Phase Metal−Organic Framework Postmodification. *J. Am. Chem. Soc.* **2020**, *142*, 242−250.
(62) Jia, M.; Su, J.; Su, P.; Li, W. Vapor-Assisted Self-Conversion of Basic Carbonates in Metal−Organic Frameworks. *Nanoscale* **2021**, *13*, 5069−5076.

(63) Mendiratta, S.; Usman, M.; Lu, K.-L. Expanding the Dimensions of Metal−Organic Framework Research towards Dielectrics. *Coord. Chem. Rev.* **2018**, *360*, 77−91.
(64) Rocío-Bautista, P.; Gutiérrez-Serpa, A.; Cruz, A. J.; Ameloot, R.; Ayala, J. H.; Afonso, A. M.; Pasán, J.; Rodríguez-Hermida, S.; Pino, V. Solid-Phase Microextraction Coatings Based on the Metal-Organic Framework ZIF-8: Ensuring Stable and Reusable Fibers. *Talanta* **2020**, *215*, 120910.
(65) Eum, K.; Hayashi, M.; De Mello, M. D.; Xue, F.; Kwon, H. T.; Tsapatsis, M. ZIF-8 Membrane Separation Performance Tuning by Vapor Phase Ligand Treatment. *Angew. Chem., Int. Ed.* **2019**, *58*, 16390−16394.
(66) Hayashi, M.; Lee, D. T.; de Mello, M. D.; Boscoboinik, J. A.; Tsapatsis, M. ZIF-8 Membrane Permselectivity Modification by Manganese(II) Acetylacetonate Vapor Treatment. *Angew. Chem., Int. Ed.* **2021**, *60*, 9316−9320.